[2] A. C. Polycarpou, M. R. Lyons, and C. A. Balanis, "Finite element analysis of MMIC waveguide structures with anisotropic substrates," *IEEE Trans. Microwave Theory Tech.*, vol. 44, pp. 1650–1663, Oct. 1996.
[3] P. Mezzanotte, M. Mongiardo, L. Roselli, R. Sorrentino, and W. Heinrich, "Analysis of packaged microwave integrated circuits by FDTD," *IEEE Trans. Microwave Theory Tech.*, vol. 42, pp. 1796–1801, Sept. 1994.
[4] S. J. Chung and L. K. Wu, "Analysis of the effects of a resistively coated upper dielectric layer on the propagation characteristics of hybrid modes in a waveguide shielded microstrip using method of lines," *IEEE Trans. Microwave Theory Tech.*, vol. MTT-41, pp. 1393–1399, May 1993.
[5] H. H. Chen and S. J. Chung, "Shielding effect of a diaphragm in a packaged microstrip circuit," *IEEE Trans. Microwave Theory Tech.*, vol. 43, pp. 1082–1086, May 1995.
[6] J. Jin, *The Finite Element Method in Electromagnetics.* New York: Wiley, 1993.
[7] S. L. Foo and P. P. Silvester, "Boundary-marching method for discontinuity analysis in waveguides of arbitrary cross section," *IEEE Trans. Microwave Theory Tech.*, vol. 40, pp. 1889–1893, Oct. 1992.
[8] R. Pregla and W. Pascher, "The method of lines," in *Numerical Techniques for Microwave and Millimeter Wave Passive Structures*, T. Ithoh, Ed. New York: Wiley, 1989, ch. 6.

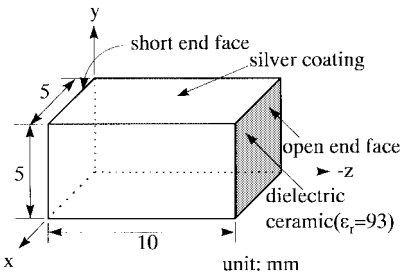

Fig. 1. Structure of the dual-mode $\lambda/4$ resonator.

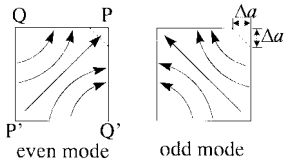

Fig. 2. Two basis modes for estimation of coupling.

Equivalent-Circuit Representation and Explanation of Attenuation Poles of a Dual-Mode Dielectric-Resonator Bandpass Filter

Ikuo Awai, Arun C. Kundu, and Takeharu Yamashita

***Abstract*— A $\lambda/4$ rectangular-waveguide resonator of square cross section filled with high-permittivity ceramics has two degenerate lowest modes. A dual-mode bandpass filter based on this structure is studied, focusing on the attenuation poles at both sides of the passband. It is described how to achieve capacitive and inductive coupling between dominant modes of a resonator of square cross section. An equivalent-circuit model is proposed, including mode coupling, excitation from the external circuit, and direct coupling between input/output (I/O) electrodes. Equivalent-circuit parameters are measured and their validity is verified using simulated result. Appearance and annihilation of the attenuation poles are successfully explained by the proposed model, and attenuation pole frequencies are controlled by shifting the I/O electrode transversely.**

***Index Terms*—Attenuation pole, dielectric resonator, dual mode, equivalent circuit.**

I. Introduction

Dual-mode resonators are one of the most effective means for miniaturizing a bandpass filter (BPF). Hence, many studies have contributed to elucidate the mechanism of coupling between dual modes and principles of fabricating a BPF [1], [2]. Attenuation poles outside of the passband, on the other hand, help to improve the skirt characteristics, resulting in further miniaturization of a BPF through reduction of the number of resonators. Though an equivalent-circuit model of an electromagnetic structure is valid only in a narrow band, it is easier to understand and gives a clear insight into the physics of the object. Thus, we will try to show the origin of attenuation poles that appear in a dual-mode two-stage BPF and try to control them based on an equivalent circuit.

The attenuation poles of a dual-mode cavity filter was explained by Zaki *et al*. [3] in an intelligible manner. However, our current work is an improved one from the following point of view: the configuration is simpler for excitation, tuning, and coupling of dual-modes, and also for the second coupling path that is essential to attenuation poles. Both types of excitation (capacitive and inductive) are possible here. Our lumped-element equivalent circuits are intuitively understandable, and the equivalent-circuit parameters are readily determined.

Manuscript received November 24, 1997; revised August 10, 1998.

The authors are with the Department of Electrical and Electronic Engineering, Yamaguchi University, Ube 755, Japan.

Publisher Item Identifier S 0018-9480(98)09051-6.

II. Coupling Between Dual Degenerate Modes

The physical structure of a directly silver-coated $\lambda/4$ dielectric waveguide resonator of square cross section, having a dimension of 5 mm × 5 mm × 10 mm, is shown in Fig. 1, where the dual modes are named as TE'_{101} and TE'_{011} [4]. We will now define new basis modes by vectorial addition and subtraction of TE'_{101} and TE'_{011} modes, naming them even and odd modes, respectively, as shown in Fig. 2.

If we add a triangular metal pattern at the corner of the OEF [2], it will make an additional current path to the resonant modes, resulting in a frequency shift in the basis modes. When the pattern is located at the corner P and/or P' of Fig. 2, it decreases inductance of the odd mode and, thus, increases the resonant frequency with little effect to the even-mode frequency. The coupling constant is simply

$$k = \frac{\left|f^{o2} - f^{e2}\right|}{f^{o2} + f^{e2}} \tag{1}$$

where f^e and f^o are the even- and odd-mode resonant frequency, respectively.

The coupling constant versus dimension of triangular metal pattern is shown in Fig. 3. From this figure, we observe that the coupling constant increases proportionally to the area of metal pattern. The validity and accuracy of this coupling method is confirmed by comparing the finite-difference time-domain (FDTD) analysis data with measured results.

An equivalent lumped-element circuit model for magnetic coupling i.e., inductive coupling between two parallel *LC* resonators, is illus-

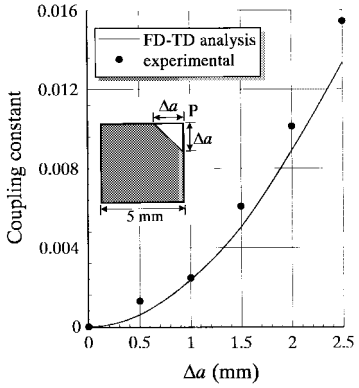

Fig. 3. Coupling constant versus dimension of triangular metal pattern at the OEF of the $\lambda/4$ resonator.

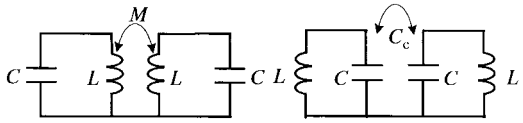

Fig. 4. Two basic lumped-element coupled resonators. (a) Inductive coupling. (b) Capacitive coupling.

trated in Fig. 4(a). We can obtain the following even- and odd-mode resonant frequency, respectively [5],

$$f^e = \frac{1}{2\pi\sqrt{(L+M)C}} \tag{2}$$

$$f^o = \frac{1}{2\pi\sqrt{(L-M)C}}. \tag{3}$$

Thus, the magnetic coupling constant $k_m = (M/L)$, which is the ratio of the coupled magnetic energy to the stored energy of the uncoupled single resonator [6]. From (2) and (3), we find that the odd-mode resonant frequency is higher than that of even-mode resonant frequency. Therefore, we can consider that the triangular metal pattern at corner P and/or P' produces inductive coupling.

Similarly, for electric (electric) coupling in Fig. 4(b), the even- and odd-mode resonant frequency becomes

$$f^e = \frac{1}{2\pi\sqrt{L(C-C_c)}} \tag{4}$$

$$f^o = \frac{1}{2\pi\sqrt{L(C+C_c)}}. \tag{5}$$

Thus, the electric coupling constant $k_e = (C_c/C)$. Here, (4) and (5) shows that the even-mode frequency is higher than that of odd-mode frequency. As a result, it can be concluded that the metal pattern at the corner Q and Q' introduces capacitive internal coupling.

III. Excitation of the Dual Modes and Direct Coupling Between I/O Electrodes

Capacitive excitation at the open-end face (OEF) and inductive excitation at the short-end face (SEF) would be most effective, as shown in Fig. 5(a) and (b) [7]. Excitation efficiency increases according to the length of the excitation electrode for each case.

Due to proximity of input/output (I/O) electrodes, a direct coupling happens between them (capacitive for Fig. 5(a) and inductive for Fig. 5(b) [8]) since the nature of coupling depends upon the nature of excitation. These additional signal paths induce attenuation poles, as will be discussed later.

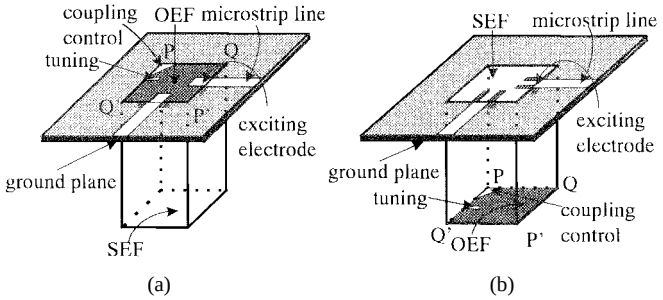

Fig. 5. Configurations of the dual-mode filter. (a) Capacitive excitation at the OEF. (b) Inductive excitation at the SEF.

IV. Equivalent-Circuit Representation of Dual-Mode BPF

A. Capacitive Excitation at the OEF

The dual-mode BPF's in Fig. 5 are made of two $\lambda/4$ resonators. It is well known that a $\lambda/4$ resonator is approximated as a parallel LC circuit around the resonant frequency. The triangular metal pattern at corner P and/or P' will provide inductive internal coupling.

The metal electrodes connected to the microstrip lines in Fig. 5(a) for capacitive excitation of the resonator will provide additional capacitor C_m, which will arise due to direct capacitive coupling between the I/O electrodes. Thus, we can easily obtain the equivalent circuit, as shown in Fig. 6(a). Here, C_e is due to the excitation electrode, G is the loss factor, and M is the mutual inductance. Now, if we simply place the metal pattern at corner Q and Q' in exchange of P and/or P', it will offer capacitive internal coupling C_c instead of M.

B. Inductive Excitation at the SEF

Configuration for inductive excitation at the SEF is shown in Fig. 5(b). Here, there will also be an additional inductance L_m that comes from the direct inductive coupling between I/O electrodes. Hence, the metal pattern at corner P and/or P' will give us the equivalent circuit of Fig. 6(b), where L_e is due to the excitation electrode. Similarly, the metal pattern at corner Q and Q' will provide a lumped-element equivalent circuit having capacitive internal coupling.

V. Measurement of the Lumped-Element Equivalent-Circuit Parameters and Simulation

When the resonator is excited at the OEF from a single port and no perturbation is provided, its equivalent circuit will be reduced to the half of Fig. 6(a), excluding C_m, as shown in Fig. 7(a). From the resonant frequency f_0 and the susceptance slope parameter, the values of C and L can be easily determined [9]. Loss factor G can be obtained from the unloaded quality factor of the resonator.

The input impedance of the mentioned circuit has a locus, as shown in Fig. 7(b). The capacitance C_e is calculated from the frequency f_1 and f_2 where the locus intersects the real axis of the Smith chart (cf. Appendix). The mutual inductance M for magnetic internal coupling [as shown in Fig. 6(b)] is easily obtained from the difference of odd- and even-mode resonant frequencies. The direct-coupling capacitance C_m is to be measured by a parallel resonance with an externally connected inductance of known values between I/O ports.

VI. Attenuation Poles

The condition for having attenuation poles at both sides of the passband is given by Konishi [10] for a two-stage BPF, shown in

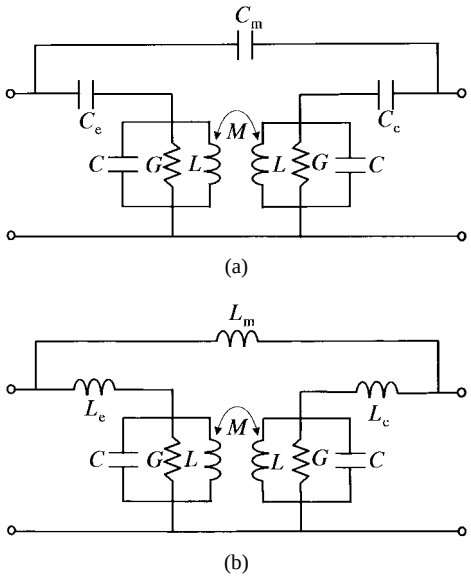

Fig. 6. Equivalent circuits of dual-mode filter. (a) Capacitive excitation at the OEF. (b) Inductive excitation at the SEF.

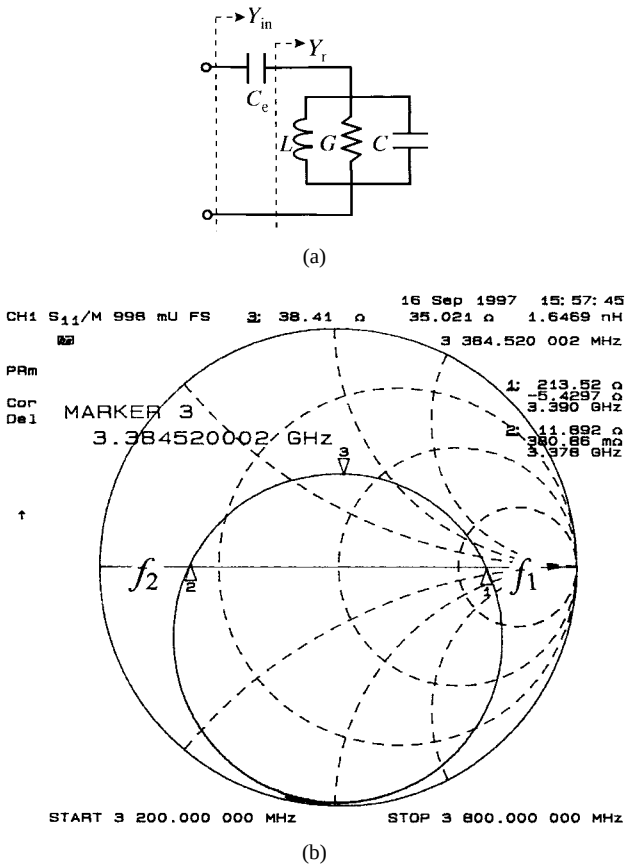

Fig. 7. Experimental setup for determination of C, L and C_e and measurement principle. (a) Equivalent circuit. (b) Locus of input impedance.

Fig. 8, as

$$b \cdot b_m < 0 \tag{6}$$

where b_m is the coupling susceptance between resonators, and b is the direct-coupling susceptance [9]. The above equation claims that the coupling between dual modes and that between I/O electrodes should be of different signs in order to have attenuation poles. Our lumped-element models are justified through simulated results by

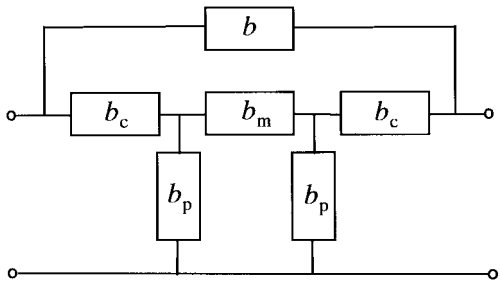

Fig. 8. Equivalent circuit for dual-mode BPF with second signal path.

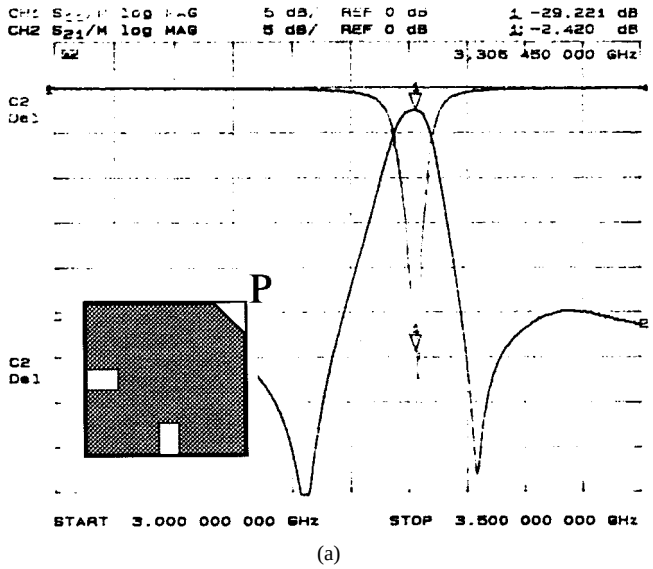

Fig. 9. Passband response of the dual-mode filter. (a) Measured response of the dual-mode filter for capacitive excitation at the OEF and metal pattern placed at corner P. (b) Simulated response ($C_m = 0.13$ pF, $C_e = 2.1$ pF, $C = 134.5$ pF, $L = 0.017$ nH, $M = 0.000\,11$ nH, $Q_0 = 580$).

comparing with the experimental results for appearance and annihilation of attenuation poles at both sides of the passband, as shown in Figs. 9–12. The equivalent-circuit parameters are determined using the procedures described in Section V.

VII. Control of Attenuation Poles

Let us consider the case of capacitive excitation at the OEF, as shown in Fig. 5(a). We could control the direct coupling between the two electrodes by shifting the position of exciting electrode transversely, which stands for change of C_m in Fig. 6(b). Fig. 13 shows the experimental result for three different positions of the exciting electrodes. As the electrodes get closer to each other, C_m increases and attenuation poles are shifted toward the center frequency [8].

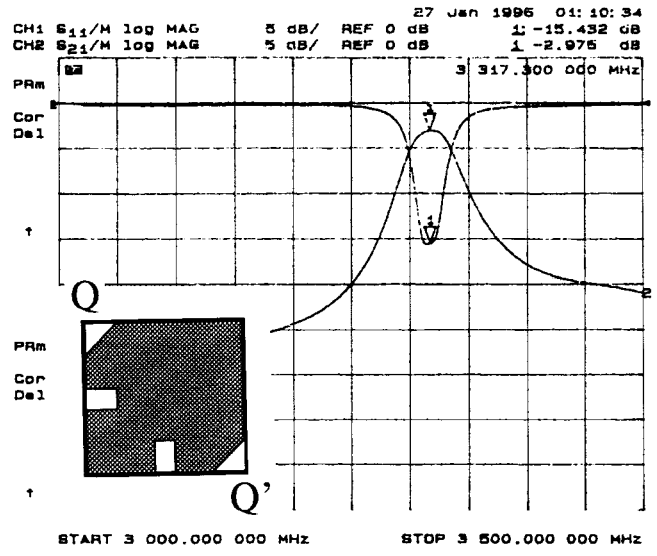

(a)

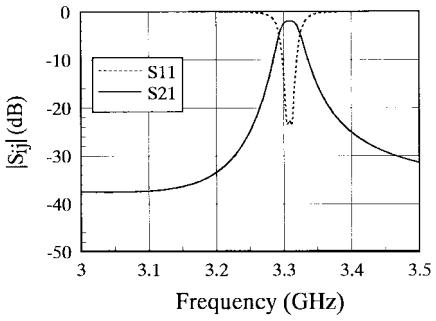

(b)

Fig. 10. Passband response of the dual-mode filter. (a) Measured response of the dual-mode filter for capacitive excitation at the OEF and metal pattern placed at corner Q and Q'. (b) Simulated response ($C_m = 0.13$ pF, $C_e = 4$ pF, $C = 135$ pF, $L = 0.017$ nH, $C_c = 0.8$ pF, $Q_0 = 580$).

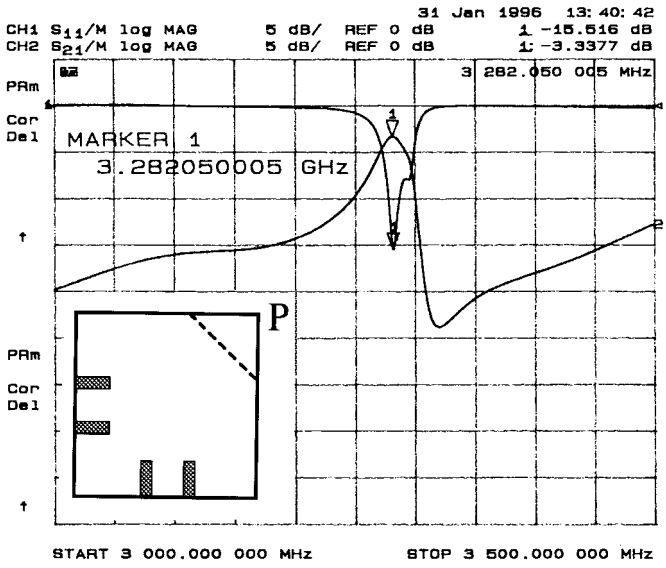

(a)

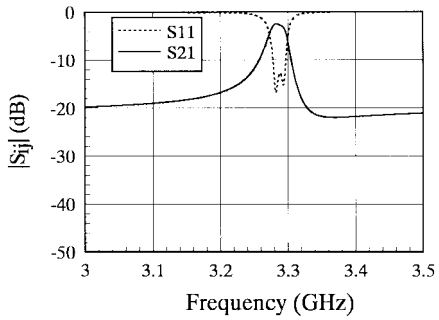

(b)

Fig. 11. Passband response of the dual-mode filter. (a) Measured response of the dual-mode filter for inductive excitation at the SEF and metal pattern placed at corner P. (b) Simulated response ($L_m = 9.25$ nH, $L_e = 1.3$ nH, $C = 136$ pF, $L = 0.0173$ nH, $M = 0.000\,08$ nH, $Q_0 = 580$).

Here, we observe that the shift of attenuation-pole frequency is not symmetric with respect to the passband frequency because when the exciting electrodes are shifted from the central position, the effect of C_m upon the upper and lower poles becomes asymmetric. Similarly, for inductive excitation at the SEF, the attenuation-pole frequencies can be controlled by changing L_m.

VIII. Conclusion

We have discovered lumped-element equivalent circuits for a dual-mode dielectric-resonator BPF, including mode coupling, excitation, and I/O electrode coupling schemes. We have also measured all the parameters of the devised equivalent circuit independently. Based on these circuits, we have elucidated the mechanism of attenuation poles at both sides of the passband in this type of BPF, and have shown an example to control the frequencies of those poles.

Appendix

Calculation of equivalent-circuit parameters in Fig. 9(a).

The susceptance of the resonator is given by

$$\begin{aligned} B_r &= (\omega C - 1/\omega L) \\ &= \omega C\left(1 - \frac{1}{\omega^2 LC}\right) \\ &= 4\pi \Delta f C \end{aligned}$$

$$\because \omega \cong \omega_0. \tag{A1}$$

Therefore,

$$(dB_r/df) = 4\pi C. \tag{A2}$$

If we draw a graph of B_r versus f around the resonant frequency from the experimental data, it will be a straight line. From the slope of this line and using (A2), one can measure the capacitance of the resonator.

L and G can be calculated as follows:

$$L = \frac{1}{\omega_0^2 C} \tag{A3}$$

$$G = \frac{\omega_0 C}{Q_0}. \tag{A4}$$

Again, from Fig. 9(a),

$$Z_{\text{in}} = \frac{1}{Y_{\text{in}}} = \frac{GB_e - j[G^2 + B_r(B_r + B_e)]}{B_e(G^2 + B_r^2)} \tag{A5}$$

where $B_e = \omega C_e$.

If we consider that the imaginary part of the numerator of (A5) is equal to zero along the real axis of the Smith chart in Fig. 9(b), we have

$$G^2 + B_r^2 + B_r B_e = 0. \tag{A6}$$

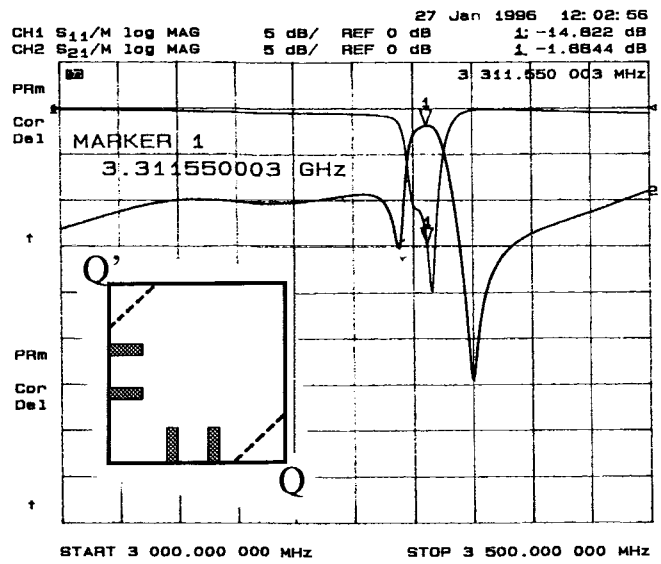

(a)

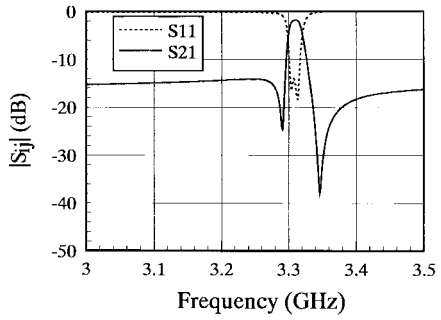

(b)

Fig. 12. Passband response of the dual-mode filter. (a) Measured response of the dual-mode filter for inductive excitation at the SEF and metal pattern placed at corner Q and Q' of the OEF. (b) Simulated response ($L_m = 7$ nH, $L_e = 1.7$ nH, $C = 135$ pF, $L = 0.017$ nH, $C_c = 0.8$ pF, $Q_0 = 580$).

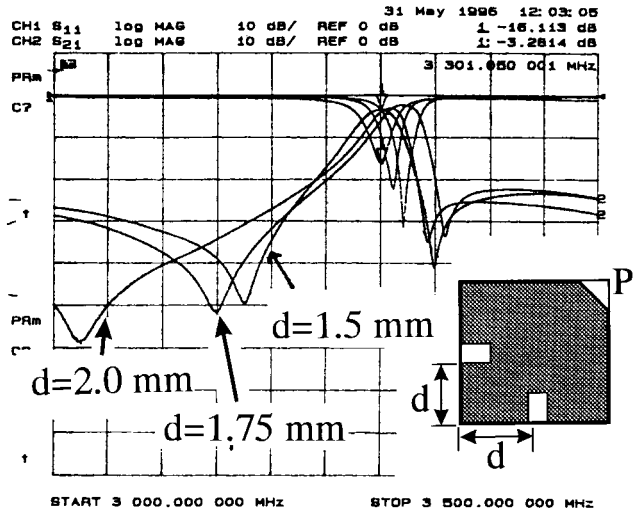

Fig. 13. Control of attenuation poles.

Now, if we substitute the values of B_r and B_e into (A6) and put $\omega = \omega_0 + \Delta\omega$, we get the following relation:

$$2C(2C + C_e)\Delta\omega^2 + 2CC_e\omega_0\Delta\omega + G^2 = 0. \tag{A7}$$

Let us suppose that $\Delta\omega_1 \& \Delta\omega_2$ are the two roots of the above quadratic equation. Hence, the locus of the frequencies crossing the real axis of the smith chart [as shown in Fig. 9(b)] can be defined by the following relations:

$$\omega_1 = \omega_0 + \Delta\omega_1$$
$$\omega_2 = \omega_0 + \Delta\omega_2$$
$$\because \omega_1 - \omega_2 = \Delta\omega_1 - \Delta\omega_2$$
$$= \frac{\omega_0}{2}\sqrt{\left(\frac{C_e}{C}\right)^2 - \left(\frac{2}{Q_0}\right)^2} \tag{A8}$$
$$\therefore \frac{C_e}{C} = \sqrt{\left[\frac{2(\omega_1 - \omega_2)}{\omega_0}\right]^2 + \left(\frac{2}{Q_0}\right)^2}. \tag{A9}$$

Hence, the parameter C_e can be calculated by using the above relation.

REFERENCES

[1] J. A. Curtis and S. J. Fiedziuszko, "Miniature dual-mode microstrip filters," in *IEEE MTT-S Symp. Dig.*, 1991, pp. 433–436.
[2] X. P. Liang, K. A. Zaki, and A. E. Atia, "Dual-mode coupling by square corner cut in resonators and filters," *IEEE Trans. Microwave Theory Tech.*, vol. 40, pp. 2294–2301, Dec. 1992.
[3] K. A. Zaki, C. Chen, and, A. E. Atia, "A circuit model of probes in dual-mode cavities," *IEEE Trans. Microwave Theory Tech.*, vol. 36, pp. 1740–1746, Dec. 1988.
[4] A. C. Kundu and I. Awai, "Resonant frequency and quality factors of a silver-coated $\lambda/4$ dielectric waveguide resonator," *IEEE Trans. Microwave Theory Tech.*, vol. 46, pp. 1124–1131, Aug. 1998.
[5] S.-W. Chen and K. A. Zaki, "A novel coupling method for dual-mode dielectric resonators and waveguide filters," *IEEE Trans. Microwave Theory Tech.*, vol. 38, pp. 1885–1893, Dec. 1990.
[6] J.-S. Hong and M. J. Lancaster, "Coupling of microstrip square open-loop resonators for cross-coupled planar microwave filters," *IEEE Trans. Microwave Theory Tech.*, vol. 44, pp. 2099–2109, Dec. 1996.
[7] I. Awai and T. Yamashita, "Coupling of dual modes in a dielectric waveguide resonator and its application to a bandpass filter," in *Proc. 25th EuMc*, Bologna, Italy, Sept. 1995, pp. 533–537.
[8] I. Awai, A. C. Kundu, and T. Yamashita, "Equivalent circuit representation and attenuation pole control of a dual-mode dielectric BPF," in *Proc. APMC*, New Delhi, India, Dec. 1996, pp. 177–180.
[9] I. Awai and T. Yamashita, "A dual-mode dielectric resonator filter with two notches," in *Proc. APMC*, Taejon, Korea, Oct. 1995, pp. 295–298.
[10] Y. Konishi, *Design and Application of Filter Circuits for Communication.* Tokyo, Japan: Sohgoh Denshi, 1994.